CONTENTS

A IMPLEMENTATION DETAILS

A.1 FINDING SPURIOUS ATTRIBUTES

We delve into our manual identification process for spurious attributes as described in Section 3.2. Following the approach outlined in (Singla & Feizi, 2021), we present a simplified version. For each category, we randomly select 5 images from the training set and generate the corresponding heatmap. We also reference external sources like Wikipedia and seek advice from ChatGPT. Using this information, we assess whether an attribute belongs to the main object or a separate background element, with options: ”Yes”, ”No”, or ”Unsure”. Finally, attributes categorized as ”No” are deemed spurious attributes. It is important to mention that unlike (Singla & Feizi, 2021), we do not conduct crowd studies. All supervision tasks are performed by the authors.

A.2 PROMPTING LLMS

We conduct a naive attempt to modify the prompting technique of LLMs to avoid generating spurious attributes in Section 3.2. We try three variant prompt templates by appending or inserting additional instructions as follows:

T1: Only focus on ___ itself.
T2: Imagine you are an expert of ___.
T3: Do not describe other than ___.

For each instruction, we position it at either the beginning or the end, yielding six combinations. Then, we employ existing attribute-based methods, *e.g.*, ArGue (Tian et al., 2024), to derive results, averaging them across all combinations.

A.3 QUERYING MLLMS

In addition to the techniques and parameters introduced in the main paper, we believe a crucial step in dealing with MLLMs is managing their outputs. Given a specified temperature, the output variance of an MLLM, particularly GPT-4V, for the same input can be significant. The responses may range from a single word to a complete paragraph, and the model may fail to follow the demonstrated formats or refuse to respond. Similar challenges have been noted in recent studies, such as DCLIP (Menon & Vondrick, 2023) and CuPL (Pratt et al., 2023), when using MLLMs or LLMs to generate attributes. In this work, we employ a simple regular expression to retain responses of suitable length and exclude those that are not formatted with bullet points. Additionally, we filter out duplicate or similar attributes. For example, between ice surface and glacier we typically randomly select only one.

A.4 CONSTRUCTING PSEUDO CATEGORIES

Here, we describe the process of constructing images targeting spurious attributes using SD (Rombach et al., 2022) or LAION-5B (Schuhmann et al., 2022). For the former, following Sus-X (Udandarao et al., 2022), we use the common checkpoint stable-diffusion-v1-4, with a guidance scale of 7.0. The diffusion step is set to 100, with a fixed output resolution of 512x512. Additionally, to ensure the diversity of the images, we use ChatGPT to generate multiple SD prompts. Specifically, we provide a vanilla prompt as an example, e.g., a photo of a mouse, and then ask GPT to rephrase the prompt in different formats. Some example generated prompts are displayed below.

P1: a 3D realistic photo of a ___
P2: a high-quality natural image of ___.
P3: a intriguing portray of ___.

It is worth noting that the prompts mentioned above are also applicable for pre-training retrieval. For LAION-5B, we select the matches with the highest average semantic similarity to these GPT-generated prompts to construct pseudo categories. This approach ensures the diversity of the retrieved images while also enhancing the reliability of semantic matching.

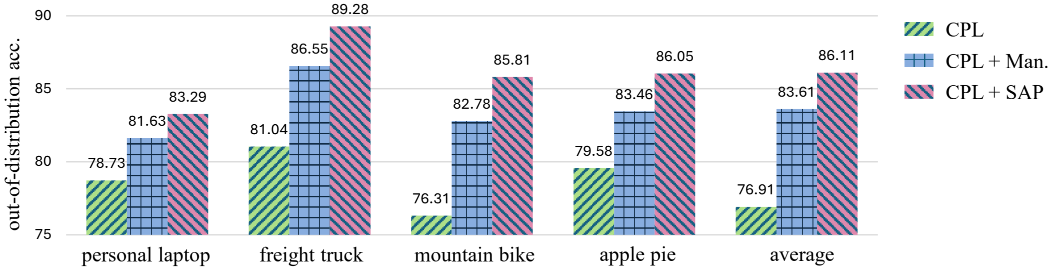

Figure 6: **The per-category out-of-distribution accuracy on domain generalization.** In this setting, based on the strong baseline CPL, we remove spurious attributes identified by manual inspection (Man.) or SAP for a specific category and compare the accuracy change on the category in the out-of-distribution datasets. All results are averaged over 4 ImageNet variants.

Category name	Spurious attributes	Average weights
Personal laptop	*mouse, coffee, charger, worktable*	77.34% / 46.73%
Freight truck	*road, traffic light, trees, street*	82.16% / 54.69%
Mountain bike	*trees, road, mountain, swamp*	74.81% / 43.02%
Apple pie	*fork, plates, dining car, tablecloth*	67.29% / 37.44%

Table 6: **The spurious attributes identified by SAP.** For each example category, we pinpoint its spurious attributes and determine the average attribute weights on model predictions using CBMs across identified spurious attributes (**Left**) and all generated attributes (**Right**).

B More Evaluation

B.1 Example Spurious Attributes

SAP quantifies the identification of spurious attributes without human supervision, offering a more precise measure of spurious correlation. This aids in effectively pinpointing attributes favored by VLMs. Table 6 showcases typical spurious attributes found by SAP, including instances like mouse frequently appearing with laptop, or fork being closely associated with apple pie. Additionally, we assess their weights on model predictions, along with the average weights of all generated attributes for reference. Notably, spurious attributes carry substantially higher weights in model decision-making compared to overall attributes, further underscoring the biased nature of VLMs.

B.2 SAP vs Human Supervision

Finding spurious attributes through human supervision (Singla & Feizi, 2021; Wong et al., 2021), while comprehensive, has significant drawbacks: 1) it incurs extremely high labor costs; 2) its strong subjectivity easily introduces false positives, where identified attributes are only present by chance. Here, we compare the performance of the proposed automatic identification method, SAP, with human supervision. We adopt domain generalization as the task and select CPL (Zhang et al., 2024b) as the baseline. For better interpretation, we remove spurious attributes from individual categories one at a time and record the change in per-category accuracy on out-of-distribution datasets. Fig. 6 depicts the results in CPL, as well as the results after removing spurious attributes through the two identification approaches. It can be seen that SAP's performance is comparable or even outperforms human supervision.

B.3 Querying with SAP at Scale

In the main paper, we address a challenging setting, specifically few-shot scenarios where training data is limited. This leads to a pertinent question: is a small number of images truly adequate for SAP to identify spurious attributes within categories? In other words, would querying more images further enhance SAP's performance? To investigate the potential of scaling up, we expand

# Query Images	1	2	4	8	16	32	64
CoCoOp	75.62	76.06	76.84	77.56	78.10	78.24	78.28
MaPLe	81.98	82.55	83.47	84.01	84.49	84.60	84.53
PromptSRC	82.59	83.35	84.13	84.72	85.46	85.63	85.68

Table 7: **The evaluation on base-to-new generalization while querying different number of images per-category.** The results are averaged across 11 datasets.

MLLM	BLIP-2	LLaVA	InternVL	GPT-4V
CoCoOp	72.28	72.79	73.14	**73.50**
MaPLe	76.20	76.83	77.25	**77.69**
PromptSRC	76.43	77.01	77.37	**77.88**

Table 8: **The evaluation on base-to-new generalization with various MLLMs.**

the training dataset from 16-shot to 256-shot and have GPT-4V query 1, 2, 4, 8, 16, 32, and 64 randomly selected images from the training shots. We evaluate the average new category accuracy on base-to-new generalization tasks across 11 datasets, comparing three typical baselines: CoCoOp, MaPLe, and PromptSRC. As shown in Table 7, despite the availability of additional shots during training, the results tend to plateau when querying with 16 images. This indicates that even with an expanded training dataset, MLLMs require only around 16 query images to capture sufficient and effective spurious attributes.

B.4 Effect of Choices of MLLMs

In previous experiments, we default our MLLM to GPT-4V. Here, we attempt to use more open-sourced MLLMs to comprehensively evaluate the robustness of our proposed method. We consider three recently popular MLLMs: BLIP-2 (Li et al., 2023), LLaVA (Liu et al., 2024), and InternVL (Chen et al., 2024). Table 8 presents the performance of these different MLLMs on base-to-new generalization tasks with 16-shot. As expected, GPT-4V, the proprietary model, achieves the best results. The next best performance is from InternVL. Conversely, BLIP-2 shows the poorest performance, which we attribute to its tendency to produce a limited vocabulary that results in overly broad core and spurious attributes.

B.5 Synthetic Generation vs Pre-training Retrieval

In previous experiments, our default approach is to utilize Stable Diffusion for constructing pseudo categories. Here, we explore an alternative method: retrieving image samples from the pre-training dataset. Table 9 illustrates the results of both approaches across several baselines. Notably, Stable Diffusion consistently outperforms retrieval from LAION-5B. This unexpected result is intriguing,

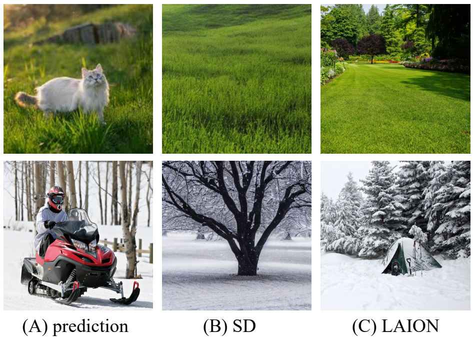

Figure 7: **Constructed images.**

	CoCoOp	KgCoOp	MaPLe	PromptSRC	CPL
SD	**76.93**	**78.51**	**80.06**	80.57	**82.87**
LAION	76.46	78.45	79.32	**80.85**	82.35

Table 9: **The comparison between synthetic generation and pre-training dataset retrieval.** We select 5 strong baselines. The results are harmonic mean of accuracy on base and new categories for base-to-new generalization.

λ	0	1	2	5	10	20
Base	83.23	**83.73**	83.64	83.15	82.41	81.53
New	74.82	76.00	77.36	**77.73**	76.60	76.89
HM	78.80	79.68	**80.38**	80.35	79.40	79.14

Table 10: **The effect of $\mathcal{L}_{pse}$ with different λ on base-to-new generalization.**

considering that pre-training images predominantly consist of real data, which one would expect to better match the style of the target category. However, the results suggest otherwise. We speculate that the complexity of real image distributions, coupled with noise attributes, may contribute to this disparity. For instance, in Fig. 7, when associating the spurious attribute snowforest with snowmobile, the top-1 match retrieved using LAION-5B includes elements such as tent and bag. These noise attributes could potentially introduce new shortcuts, complicating the model's ability to differentiate spurious attributes from the target category.

B.6 Balancing the Effect of SAS

Table 10 examines the balancing effect between $\mathcal{L}_{pse}$ and primary learning objectives in existing work in terms of λ. The best trade-off is observed at around $\lambda = 2$. As λ increases further, it begins to neglect the primary objectives of the baselines, leading to a decline in base accuracy. Notably, these results are averaged across multiple baselines. In fact, for distinct baselines, we suggest exploring optimal values individually due to their respective learning characteristics.

B.7 Quantitative Comparison with Related Work

In the main text, we primarily demonstrate the effectiveness of SAS in complementing existing PEFT methods. Here, we further substantiate the advantages of SAS by comparing it with other state-of-the-art spurious correlation mitigation approaches. We evaluate a typical property of VLMs, group robustness, which indicates the invariance of VLMs under different associations between labels and attributes. For the baselines, we consider C-Adapter (Zhang & Ré, 2022) and CFR (You et al., 2024),

Method	Waterbirds			CelebA			BREEDS			CIFAR-10.02		
Accuracy (%)	WG	Avg	Gap	WG	Avg	Gap	WG	Avg	Gap	WG	Avg	Gap
Zero-shot	25.7	87.3	61.6	62.1	71.9	9.8	4.0	86.6	82.6	72.0	93.2	21.2
RoboShot	45.2	79.9	34.7	82.6	85.5	2.9	56.4	80.3	23.9	79.1	95.6	16.5
Linear Probe	65.9	97.6	31.7	28.3	94.7	66.4	84.0	98.6	14.6	87.5	96.1	8.6
C-Adapter	86.9	96.2	9.3	84.6	90.4	5.8	80.0	97.5	17.5	82.2	96.1	13.9
DISC	88.7	93.8	5.1	82.0	92.5	10.5	86.3	95.8	9.5	84.7	94.3	9.6
CFR	88.2	96.7	8.5	84.7	87.8	3.1	85.0	96.1	11.1	**89.1**	92.5	3.4
SAS	**89.7**	96.3	6.6	**87.4**	91.1	3.7	**87.8**	96.4	8.6	88.5	95.2	6.7

Table 11: **The group robustness evaluation of SAS and other spurious correlation mitigation methods.** We report worst-group accuracy (WG), average-group accuracy (Avg) and the gap between. Note that RoboShot is a zero-shot calibration method, while other approaches are training-required.

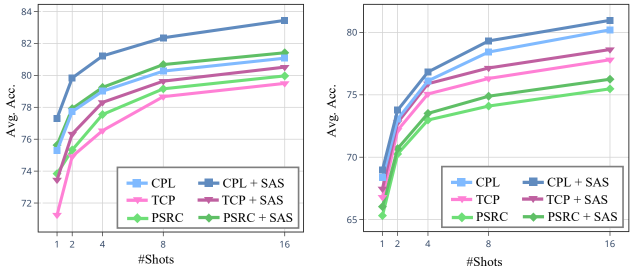

(A) base-to-new generalization (B) standard few-shot classification

Figure 8: **The results varying shots on base-to-new generalization and few-shot classifcation.**

where spurious attributes are assumed to be unknown. We also include RoboShot (Adila et al., 2023) and DISC (Wu et al., 2023), where, similar to our approach, spurious concepts are identified and used for precise mitigation. By default, we configure SAS to optimize only the learnable textual prompt, *i.e.*, CoOp (Zhou et al., 2022a). It is worth noting that RoboShot (Adila et al., 2023) is a zero-shot approach that calibrates pre-trained embeddings. Following Zhang & Ré (2022), we consider four datasets with group annotations: Waterbirds (Sagawa et al., 2019), CelebA (Liu et al., 2018), BREEDS Living-17 (Santurkar et al., 2020), and CIFAR-10.02 (Krizhevsky et al., 2009). In Table 11, average-group accuracy, worst-group accuracy, and their gap are reported. It can be observed that SAS achieves a new state-of-the-art in worst-group accuracy across most datasets without excessively compromising average-group accuracy.

B.8 Generalization under Limited Shots

We consider generalization capability in extreme cases, where the shots are further limited, *i.e.*, 1/2/4/8 shots. It is noteworthy that in this scenario, limitations arise from both the insufficient amount of data and the impact on SAP's precision to identify spurious attributes, further affecting SAS performance. We select three strong baselines, encompassing PromptSRC (Khattak et al., 2023b), TCP (Yao et al., 2024) and CPL (Zhang et al., 2024b). Fig. 8 (A) shows the results of combining SAS on base-to-new generalization across different shot settings. It can be seen that the results consistently outperform the original baselines, even only one shot is given.

B.9 Standard Few-shot Classification

We consider the standard scenario where test and training samples originate from the same dataset distribution. Fig. 8 (B) illustrates the results in standard few-shot classification. Notably, integrating SAS does not compromise in-distribution accuracy; instead, it shows a slight and consistent improvement.

B.10 Discussion of Hyperparameter Sensitivity

Although we observe the state-of-the-art performance of SAS in the main context, an important aspect, hyperparameter sensitivity, still requires discussion. For the newly introduced hyperparameters in SAS, such as λ and γ, their impact on the results has been examined in previous ablation experiments. These experiments reveal that while an optimal value is preferred, SAS is not overly sensitive to these hyperparameters and consistently provides stable improvements within a certain range.

Regarding training hyperparameters such as learning rate and batch size, recent studies (Silva-Rodriguez et al., 2024) have found that some adaptation methods heavily rely on these hyperparameters in few-shot scenarios, complicating practical deployment. In contrast, as shown in Fig. 3 of the main paper, although SAS uses different training hyperparameters for different baselines as specified in the original papers, it consistently achieves gains, demonstrating its robustness to hyperparameters.

Training Data	CoCoOp	MaPLe	PromptSRC	Average
16-shot main	70.05	75.39	73.78	72.94
32-shot main	71.12	76.37	75.52	74.34
16-shot main + 16-shot pseudo main	70.34	75.80	74.46	73.53
16-shot main + 16-shot pseudo spurious (ours)	**73.50**	**77.69**	**77.88**	**76.36**

Table 12: **The ablation study on the performance gains**. We introduce two baselines, where the first incorporates additional data from the training set (32-shot main), and the second involves vanilla constructed data from pseudo categories mirroring the main categories (16-shot main + 16-shot pseudo main). In contrast, the pseudo categories of our method feature spurious attributes (16-shot main + 16-shot pseudo spurious)

B.11 Ablation on Performance Gains

In the main paper, we verify the effectiveness of SAS and explore the contribution of spurious attributes to its performance. To further confirm that the performance gains are primarily due to the model's enhanced robustness to spurious attributes rather than additional data, here we conduct a simple ablation study. Specifically, in addition to the proposed method, we design two baselines. In the first baseline, we consider additional data directly from the original dataset featuring the main objects, where we extend the training data from 16 shots to 32 shots (32-shot main). In the second baseline, we involve additional data generated by pseudo categories, where instead of featuring spurious attributes, these pseudo categories are the same as the main categories, i.e., vanilla constructed data (16-shot main + 16-shot pseudo main). In contrast to the first two baselines, our approach creates pseudo categories based on spurious attributes (16-shot main + 16-shot pseudo spurious). For fairness, we ensure that the amount of training data is identical between the two baselines and our approach. We select three typical methods for comparison, including CoCoOp (Zhou et al., 2022b), MaPLe (Khattak et al., 2023a), and PromptSRC (Khattak et al., 2023b), and evaluate them on the base-to-new generalization task. All results are averaged across 11 datasets.

As shown in Table 12, generating additional data using spurious attributes significantly outperforms vanilla constructed data for main categories (76.36% vs 73.53%). Furthermore, our proposed method even exceeds the performance of the 32-shot main (76.36% vs 74.34%). It is important to note that this comparison is not entirely fair for our method, as the latter relies on more labeled data from the original training set. This further suggests that the performance gains are primarily driven by the model's enhanced robustness to spurious attributes, rather than merely the increased training data.

B.12 More Visualization Examples

In Fig. 5, we present the saliency maps for some typical categories with and without SAS. For completeness, we provide more examples here. As shown in Fig. 9, SAS consistently reduces VLMs' bias towards spurious cues across various categories, enabling a greater focus on the main objects.

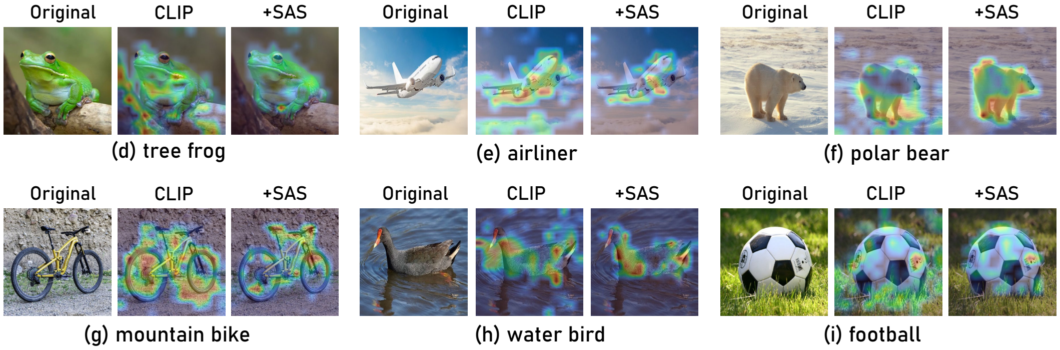

Figure 9: **More saliency map visualization with and without SAS**.

Model	CoCoOp	MaPLe	PromptSRC	Average
BLIP	68.81	72.32	72.62	70.58
BLIP + SAS	70.54	74.35	73.97	72.95
CLIPA-v2	70.28	73.40	74.52	72.73
CLIPA-v2 + SAS	72.42	74.88	77.08	74.79
EVA-CLIP	72.75	77.58	76.13	75.49
EVA-CLIP + SAS	74.60	**77.92**	77.82	76.78
SigLIP	74.99	73.78	78.64	75.80
SigLIP + SAS	**76.41**	75.26	**79.87**	**77.18**

Table 13: **The evaluation results of SAS on other VLMs**. We consider four representative VLMs including BLIP, CLIPA-v2, EVA-CLIP and SigLIP.

Method	Flowers102	Food101	FGVCAircraft	StanfordCars	Average Time
CoCoOp	10m48s	18m34s	8m02s	12m46s	12m32s
+ SAS	13m14s	24m07s	13m36s	17m08s	17m01s
+ selective trick	11m03s	20m45s	10m23s	14m55s	14m16s
PromptSRC	6m25s	15m09s	5m44s	9m36s	9m13s
+ SAS	8m26s	18m21s	7m11s	12m04s	11m30s
+ selective trick	6m58s	16m22s	6m35s	10m20s	10m03s

Table 14: **The training efficiency of SAS and selective optimization on other datasets**.

For example, for the tree frog, SAS reduces VLMs' reliance on tree branches, while for the airliner, the typical spurious attributes are sky or clouds, and the application of SAS alleviates the model's bias towards these elements.

B.13 More Vision-Language Models

For completeness, here we extend the evaluation of SAS to additional VLMs other than CLIP. Specifically, we select four typical VLMs encompassing BLIP (Li et al., 2022), CLIPA-v2 (Li et al., 2024), EVA-CLIP (Sun et al., 2023) and SigLIP (Zhai et al., 2023). We record the results on base-to-new generalization, where the setting is consistent with the main paper. As demonstrated in Table 13, our proposed method, SAS, consistently yields performance gains across a range of VLMs, extending beyond just CLIP.

B.14 Computational Efficiency and Cost

In this section, we present the computational and time costs of the proposed method, accompanied by a thorough analysis.

The cost of training. In the main paper, we present the training time of SAS and the proposed selective optimization trick on ImageNet. Here, furthermore, we provide time statistics for other datasets. The time is measured as the runtime of the training script based on the implementation of CoOp (Zhou et al., 2022a). As shown in Table 14, for most datasets, the integration of SAS only increases the training time by approximately 3 to 5 minutes, while selective optimization further reduces this time to a negligible amount. In fact, the selective optimization trick is proposed to address large-scale datasets, such as ImageNet, which contains 1000 categories. For regular datasets ($\sim$ 100 categories), the time consumption of SAS is fully acceptable.

The cost of diffusion generation. Here, we provide the estimated inference time required to construct pseudo categories through Stable Diffusion for each dataset. As shown in Table 15, the total inference time is proportional to the size of the dataset, particularly the number of categories involved. For most datasets, the inference time is under half an hour, and the entire inference process

Dataset	Caltech	Pets	Cars	Flowers	Food	Aircraft	SUN	DTD	EuroSAT	UCF	INet
Time	25min	10min	45min	30min	25min	30min	90min	15min	5min	25min	3h50min

Table 15: **The diffusion inference time for each dataset**.

Dataset	Caltech	Pets	Cars	Flowers	Food	Aircraft	SUN	DTD	EuroSAT	UCF	INet
Time	10min	10min	25min	10min	10min	10min	35min	5min	3min	10min	1h30min

Table 16: **The GPT prompting time for each dataset**.

can be completed within half a day. It is important to note that this is a one-time operation, and no additional inference is needed during subsequent training.

The cost of GPT prompting. In our method, a key step is identifying the spurious attributes within each category, which we accomplish by prompting MLLMs, i.e., GPT. Here we provide the time cost of this process along with a thorough analysis. Specifically, to enhance efficiency, we employ batch inference as implemented in Menon & Vondrick (2023), where multiple queries can be processed concurrently, which significantly reduces the inference time for GPT. As shown in Table 16, the GPT inference time for most datasets is under 10 minutes. The complete inference process takes approximately three hours, which is also a one-time operation that does not need to be repeated thereafter. It is worth noting that upon obtaining the responses, we need to perform post-processing such as filtering and selection to determine valid attributes, as detailed in Section A.3, which may require additional time.

B.15 More Modalities and Tasks

To assess the transferability of our method to other modalities or tasks, we explore video recognition and leave more tasks, such as language reasoning, for future work. Specifically, we choose ViFi-CLIP (Rasheed et al., 2023), a fully fine-tuned CLIP model tailored for video understanding. ViFi-CLIP employs a training framework similar to CLIP, incorporating a temporal pooling layer to derive video representations from multiple frames. Following the base-to-new generalization setting in Rasheed et al. (2023), we evaluate video-level generalization performance on four video datasets: K-400 (Kay et al., 2017), HMDB-51 (Kuehne et al., 2011), UCF-101 (Soomro, 2012), and SSv2 (Goyal et al., 2017). As in the main paper, we select three representative baseline methods: CoCoOp (Zhou et al., 2022b), MaPLe (Khattak et al., 2023a), and PromptSRC (Khattak et al., 2023b). Since ViFi-CLIP shares its architecture with CLIP, these methods can be easily transferred to ViFi-CLIP, which has been implemented by Khattak et al. (2023b). We incorporate the proposed method, `SAS`, into these baselines to verify its effectiveness by contrasting spurious attributes with each frame of the video. We record the new category accuracy for each dataset which directly reflects the generalization performance on unseen categories. As shown in Table 17, despite the input modalities shifting from images to videos, `SAS` consistently delivers performance gains across all

Method	K-400	HMDB-51	UCF-101	SSv2
ViFiCLIP	61.10	53.30	67.70	12.10
CoCoOp	64.70	54.41	68.21	14.24
CoCoOp + `SAS`	66.39	56.64	70.40	16.01
MaPLe	64.52	58.23	70.73	14.74
MaPLe + `SAS`	66.42	59.32	72.66	16.40
PromptSRC	68.31	62.38	76.79	17.22
PromptSRC + `SAS`	**70.23**	**64.70**	**79.31**	**18.95**

Table 17: **The evaluation results of `SAS` on four video datasets**. The training is based on ViFi-CLIP, a fully fine-tuned CLIP model for video reasoning.

Method	ImageNet	Flowers102	SUN397	FGVCAircraft	StanfordCars
MMA	71.00	75.93	78.57	36.33	73.10
MMA + SAS	72.61	77.27	**80.19**	**37.85**	75.46
DMN	72.28	78.49	77.32	32.60	74.22
DMN + SAS	**73.34**	**80.17**	79.74	35.38	**76.30**

Table 18: **The evaluation of SAS on other baselines**. We include two recently proposed approaches, including MMA and DMN.

Step	Flowers102		Food101		FGVCAircraft		StanfordCars		Average	
	Acc	Time	Acc	Time	Acc	Time	Acc	Time	Acc	Time
25	72.24	10min	91.18	6min	27.23	8min	73.55	13min	66.05	9min
50	72.85	15min	91.96	11min	**28.41**	14min	74.67	23min	66.97	16min
75	72.81	22min	**92.28**	18min	28.19	24min	74.82	31min	67.02	24min
100	**72.99**	28min	92.12	26min	28.30	31min	**74.96**	40min	**67.09**	31min

Table 19: **The performance of SAS and diffusion time with different number of diffusion steps.**

datasets, proving it to be an effective plug-and-play method that can be generalized to more complex modalities and tasks.

B.16 Evaluation on More Baselines

For completeness, here we evaluate our method on the two recently proposed works. Specifically, we select MMA (Yang et al., 2024) and DMN (Zhang et al., 2024a). For the former, we train the newly introduced adapters in the deep layers that bridge the text and image representations, following their setting and implementation. For the latter, we optimize its memory projection functions and incorporate both the static and dynamic memory networks, which is the strongest variant according to their paper. We select the base-to-new generalization task, as illustrated in Section 4, and record the new category accuracy, which directly reflects the generalization performance. As shown in Table 18, SAS consistently improves performance on both methods, demonstrating its complementarity.

B.17 Ablation on Diffusion Steps

Considering the computations introduced by diffusion in generating images, here we perform an ablation study on the efficiency of diffusion inference. Specifically, we vary the number of diffusion steps, which is the key hyperparameter influencing the inference time. Intuitively, fewer steps are more efficient yet yield lower image quality, while more steps ensure image fidelity but require more computation. We select CoCoOp as the baseline and record the new category accuracy on base-to-new generalization. As shown in Table 19, by default, we use 100 steps throughout the paper as described in Section A.4, which requires an average of 31 minutes to generate images per dataset. Here we try fewer steps, such as 50, and observe that the time required for diffusion nearly halves (31min → 16min) with minimal degradation in performance (67.09 → 66.97). However, while the number of steps is further reduced to 25, there is a dramatic performance drop (66.97 → 66.05), possibly due to the decline in image quality. This suggests we may safely adjust the number of steps from 100 to 50, which halves the required time with minimal accuracy loss, significantly improving the efficiency of SAS.

Method	ImageNet	Caltech101	OxfordPets	StanfordCars	DTD	EuroSAT	ImageNet-A	Average
CLIP	66.54	94.62	90.41	64.69	44.84	47.50	49.32	65.42
DCLIP	68.52	95.48	91.88	65.70	45.52	49.08	49.88	66.58
DCLIP - SA	67.67	94.76	91.31	64.79	45.06	47.92	49.30	65.83
CuPL	69.99	96.51	92.62	66.91	47.32	50.33	50.14	67.69
CuPL - SA	68.70	95.89	92.38	65.66	46.06	49.58	49.28	66.79

Table 20: **The zero-shot accuracy before and after removing spurious attributes.** The model is evaluated on 2 generic datasets (ImageNet (Deng et al., 2009), Caltech101 (Fei-Fei et al., 2004)), 2 fine-grained datasets (OxfordPets (Parkhi et al., 2012), StanfordCars (Krause et al., 2013)), 2 specialized datasets (DTD (Cimpoi et al., 2014), EuroSAT (Helber et al., 2019)) and 1 adversarial dataset (ImageNet-A (Hendrycks et al., 2021)).

C FURTHER EXPLORATION

C.1 SPURIOUS ATTRIBUTES FOR ZERO-SHOT RECOGNITION

The primary takeaway of this paper is the unbalanced treatment of various semantic attributes by VLMs, which extends beyond the generalization task and suggests that the language encoder of VLMs may allocate distinct attention to different tokens. We examine a typical example: zero-shot recognition, where attributes are directly utilized to make predictions without training. We consider three baselines: CLIP (Radford et al., 2021), DCLIP (Menon & Vondrick, 2023), and CuPL (Pratt et al., 2023). The latter two employ LLMs to generate attributes and enhance zero-shot accuracy. In a manner similar to the previous motivational study, we remove identified spurious attributes from the existing baselines and record the accuracy before and after this intervention. Table 20 presents the results before and after removal. We observe a significant drop in accuracy for the baselines (from 63.23% to 62.49% for DCLIP and from 64.34% to 63.45% for CuPL), with DCLIP almost reverting to the performance of vanilla CLIP (62.49% vs. 62.07%). This indicates that 1) similar to the generalization task, zero-shot recognition is also dominated by spurious attributes, nearly ignoring the presence of other generated attributes; and 2) spurious attributes, in a sense, improve zero-shot performance on natural datasets by scaling up the model's inherent bias.

C.2 SELECTIVE OPTIMIZATION TRICK

SAS introduces a subsidiary task that includes constructed pseudo categories and auxiliary learning objectives. With an increasing number of spurious attributes, a large number of pseudo categories are introduced, significantly increasing computational costs. To tackle this challenge, we introduce a strategy that selectively optimizes partial target categories with a heavy bias towards spurious attributes. In other words, we only mitigate the influence of spurious attributes on categories that overly rely on them. To identify these categories, we propose Spurious Correlation Ratio (SCR). SCR is calculated as the ratio of the average weights of spurious attributes to the average weights of all attributes, as exemplified in the rightmost column of Table 6. A higher SCR indicates that the prediction of the corresponding category relies more on spurious attributes. In implementing this trick, we empirically select only the top 10% of categories ranked by SCR for optimization. To verify the trick, we choose two time-intensive baselines, CoCoOp (Zhou et al., 2022b) and PromptSRC (Khattak et al., 2023b), for comparison. CoCoOp's training is slow due to its instance-conditioned mechanism, while PromptSRC adds three extra learning objectives to the original cross-entropy loss. To emphasize the results, we conduct evaluation on the base-to-new generalization task using ImageNet (Deng et al., 2009) and record both training time and harmonic mean accuracy. Table 5 in the main paper illustrates the trade-off between effectiveness and efficiency with SAS and the proposed trick. It is evident that integrated with selective optimization, the required time is significantly reduced compared to the original SAS. For instance, on PromptSRC, it only adds 9 minutes of training time while preserving most of the performance gains.

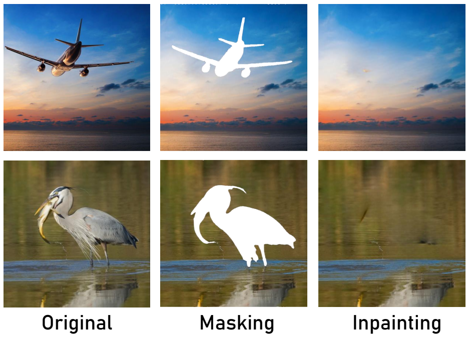

Figure 10: **The constructed categories with masking and inpainting.** For the former, we directly mask the primary object with SAM (Kirillov et al., 2023), whereas for the latter, we further use RePaint (Lugmayr et al., 2022) to fill in the missing parts. We compare the performance between the pseudo categories constructed with masking, inpainting and our synthesis method.

C.3 Variants of SAS

In the main paper, SAS primarily constructs pseudo categories using synthetic or pre-trained data, which has proven effective. Here, we consider two simple yet direct variants: 1) instead of utilizing spurious attributes to create new data, we directly mask the main object in the original images and use these as the corresponding pseudo categories, termed SAS-masking; 2) upon masking, we fill the masked area through in-painting, termed SAS-inpainting. Fig. 10 displays some example images of pseudo categories by these two variants. The motivation here is to enhance VLMs' awareness of core attributes by contrasting target categories with their corresponding images that lack main objects. We refer to the original approach as SAS-synthesis, where pseudo categories are constructed with SD-synthesized images. Table 21 presents the performance of the three methods, showing that both variants perform worse than SAS-synthesis. We speculate that this is because 1) masking or in-painting significantly reduces image fidelity; and 2) this approach introduces excessive noise attributes, thereby forming a new set of spurious attributes for VLMs to learn.

C.4 Non-semantic Spurious Attribute

In the evaluated datasets, including previous work on measuring group robustness (Zhang & Ré, 2022; Adila et al., 2023), most spurious attributes are semantically related, wherein the attribute and label exhibit a natural association, *e.g.*, water and water bird. In this study, we extend our exploration to non-semantic attributes, where the association between the attribute and label is artificially constructed. We implement a straightforward color-shifting experiment using ColoredMNIST. This dataset comprises 10 classes, each representing a digit; however, instead of the standard black background in MNIST, each digit class features a distinctly colored background. Each color demonstrates a strong spurious correlation with its corresponding digit, effectively serving as a spurious attribute. Fig. 11 illustrates examples from ColoredMNIST. We employ GPT-4V to identify these non-semantic spurious attributes, resulting in descriptors such as green background and pure yellow background. We evaluate SAS on the test set of ColoredMNIST, where the color backgrounds are randomized across labels. As shown in Table 22, SAS significantly enhances VLMs'

Method	CoCoOp	MaPLe	PromptSRC
SAS-masking	71.08	74.53	75.39
SAS-inpainting	72.95	76.81	77.04
SAS-synthesis	**73.50**	**77.69**	**77.88**

Table 21: **The evaluation on base-to-new generalization with two SAS variants.**

Method	CoCoOp	MaPLe	PromptSRC
w/o SAS	72.47	75.89	74.08
w/ SAS	84.70	88.27	87.48

Table 22: **The evaluation on ColoredMNIST with and without SAS.**

robustness to color shifting, indicating that MLLMs may capture non-semantic attributes in images, and SAS effectively leverages these attributes to improve generalization.

C.5 Limitation and Failure Cases

In SAP, the primary limitation stems from the necessity of having available images. Previous approaches to generating visual attributes only require textual information, *e.g.*, category names. The underlying assumption is that the generated attributes would be dataset-agnostic. For example, attributes like headlights, doors, or wheels for the category vehicle are assumed to be consistent across datasets. However, spurious attributes do not adhere to this assumption; they are contingent on the specific characteristics of the dataset. For instance, vehicle images in different datasets might be taken on a highway or in a parking lot, resulting in vastly different spurious attributes. This highlights the need for visual information from the dataset itself to accurately identify spurious attributes.

For SAS, the main concern still lies in efficiency. While the use of synthetic or pre-training images has been employed to address data scarcity in many recent works, such as SuS-X (Udandarao et al., 2022) and Real-Prompt (Parashar et al., 2024), these methods inevitably introduce additional computational overhead. The inference of Stable Diffusion (Rombach et al., 2022), relative to its large data requirements, is not particularly fast, and retrieval requires finding top-k matches from a huge pre-training dataset (Schuhmann et al., 2022), both of which have efficiency bottlenecks. While selective optimization tricks can minimize computational burdens as much as possible, they come at the cost of accuracy.

C.6 More Related Works

Retrieval-Augmented Generation. RAG is proposed essentially to address the insufficiency or lack of desired data. For example, Long et al. (2022) improves long-tail recognition performance by retrieving text representations for tail classes. Similarly, Parashar et al. (2024) enhances VLMs' tail accuracy by identifying and retrieving high-frequency text synonyms corresponding to tail names from the training set. Furthermore, Udandarao et al. (2022) mitigates data sparsity issues by retrieving external images through class names for data augmentation. Sharing motivations with previous work, we construct pseudo categories featuring spurious attributes through retrieval, thereby enhancing the model's robustness to these attributes. Nevertheless, beyond retrieval, we also explore data synthesis. In Section B.5, we compare the performance of our method using synthesized and retrieved data, empirically concluding that synthesized data yields greater accuracy gains. Compared to retrieval, synthesis can offer more tailored and precise scenarios and objects, which may be more suitable for our method given the diverse identified attributes.

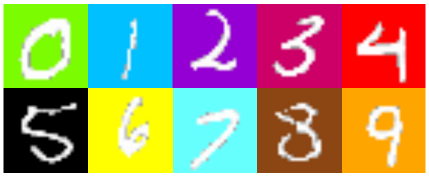

Figure 11: **ColoredMNIST.**

D Broader Societal Impacts

Our work has positive societal impacts. As illustrated in Fig. 5 of the main paper, VLMs may exhibit bias by associating harmful spurious attributes with target categories. For instance, when recognizing street sign, VLMs often rely excessively on concepts like street and road. This non-robust visual perception may lead to severe consequences in real-world applications, particularly in autonomous driving. The introduction of SAP can effectively identify such harmful attributes and even create a spurious attribute pool for specific applications, helping to determine situations where performance is compromised. Meanwhile, SAS provides an effective approach to suppress the influence of spurious attributes in VLMs, significantly enhancing the model's robustness against these attributes, including protected ones such as gender and race. Currently, we have not identified negative societal impacts of this work. However, due to objective factors, such as the availability of datasets and baselines' code, this will need to be further discussed in the future.

E Supplementary Results

E.1 Constructed Images

In Fig. 12, we provide more constructed images by SAS, with Stable Diffusion and retrieval from LAION-5B, respectively.

E.2 Spurious Attribute Statistics

Here, we present the spurious attribute statistics for the evaluated datasets. Specifically, we report the proportion of images containing one or more spurious attributes identified by SAS across 11 datasets, as shown in Table 23. The data reveals that for most datasets, over 50% of images contain spurious attributes, highlighting the biased nature of these datasets and the consequent spurious correlations learned by VLMs.

E.3 Motivational Results

Given the enhanced generalization performance of VLMs before and after removing spurious attributes in Table 1 of the main paper, to further illustrate the impact of spurious attributes, here we present the improvement of the models on the counter group in Table 24. It can be observed that the accuracy of VLMs on the counter group shows a more significant improvement, up to 9% on the unseen categories.

E.4 Numerical Main Results

Here we quantitatively demonstrate the main results as depicted in Fig. 3 of the main paper. Table 25 and Table 26 present the numerical results of base-to-new generalization, cross-dataset transfer, and domain generalization, respectively.

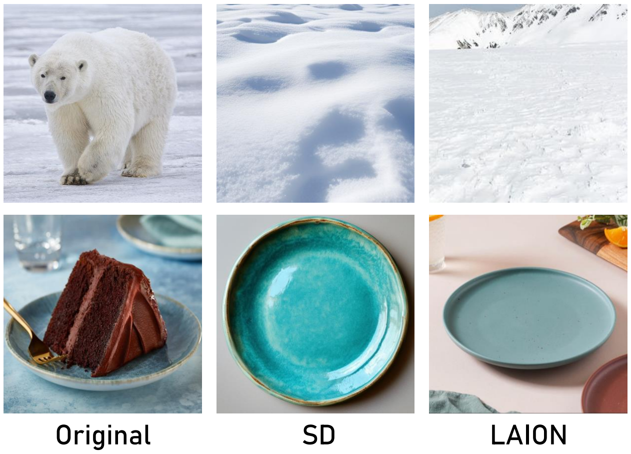

Figure 12: **More examples of generated and retrieved images with Stable Diffusion (SD) and LAION, respectively.** The category above is polar bear, with the primary spurious attribute being *snow-covered ground*. The category below is chocolate cake, where one of the spurious attributes is the *dinner plate*.

Dataset	Images with spurious attributes (%)
ImageNet	62.48
Caltech101	58.22
OxfordPets	73.54
StanfordCars	69.92
Flowers102	63.50
Food101	54.59
FGVCAircraft	47.97
SUN397	52.20
DTD	42.68
EuroSAT	47.90
UCF101	71.57

Table 23: **The proportion of images containing one or more spurious attributes of 11 datasets.**

Method	FGVCAircraft			SUN397			Flowers102			DTD			Average		
	Base	New	SR	Base	New	SR	Base	New	SR	Base	New	SR	Base	New	SR
CPL	29.25	24.80	5.43	63.47	54.74	6.61	76.98	60.77	5.71	68.93	43.14	5.13	59.66	45.86	5.72
CPL - SA	**32.42**	**31.34**	—	64.81	60.35	—	**78.35**	**69.80**	—	71.26	**52.65**	—	61.71	**53.54**	—
ArGue	27.24	21.92	5.13	65.23	57.44	6.45	72.26	59.32	6.69	70.77	40.12	5.97	58.87	44.70	6.06
ArGue*	27.92	23.83	4.86	65.99	58.21	6.11	72.87	60.49	6.44	71.29	41.28	5.62	61.27	45.95	5.76
ArGue - SA	30.71	29.20	—	**67.90**	**63.68**	—	74.68	66.45	—	**73.70**	50.19	—	**61.75**	52.38	—

Table 24: **The results on the counter group in base-to-new generalization before and after removing spurious attributes (SA) from the pool.** We extract the counter group for both the base and new categories where spurious cues are removed. It can be observed that the accuracy of VLMs improves after removing spurious attributes in this context.

Method	ImageNet		Caltech		OxfordPets		Cars		Flowers		Food		Aircraft		SUN		DTD		EuroSAT		UCF	
	Base	New	Base	New	Base	New	Base	New	Base	New	Base	New	Base	New	Base	New	Base	New	Base	New	Base	New
CLIP	72.43	68.14	96.84	94.0	91.17	97.26	63.37	74.89	72.08	77.80	90.10	91.22	27.19	36.29	69.36	75.35	53.24	59.90	56.48	64.05	70.53	77.50
CoCoOp	75.98	70.43	97.96	93.81	95.20	97.69	70.49	73.59	94.87	71.75	90.70	91.29	33.41	23.71	79.74	76.86	77.01	56.00	87.49	60.04	82.33	73.45
+ SAS	76.40	71.38	97.33	94.62	95.73	97.80	70.70	74.96	95.17	72.99	90.58	92.12	34.06	28.30	80.40	79.67	76.87	57.73	87.77	63.61	82.57	75.66
KgCoOp	75.83	69.96	97.72	94.39	94.65	97.76	71.76	75.04	95.00	74.73	90.50	91.70	36.21	33.55	80.29	76.53	77.55	54.99	85.64	64.34	82.89	76.67
+ SAS	75.78	71.24	97.96	95.40	95.43	98.67	71.46	75.93	95.51	75.86	90.69	92.03	36.93	36.20	80.80	79.02	77.89	60.30	85.78	73.73	83.38	78.94
MaPLe	76.66	70.54	97.74	94.36	95.43	97.76	72.94	74.00	95.92	72.46	90.71	92.05	37.44	35.61	80.82	78.70	80.36	59.18	94.07	73.23	83.00	78.66
+ SAS	76.69	70.82	97.92	95.35	95.88	98.47	73.16	75.46	95.93	76.74	91.41	92.47	37.87	39.68	81.30	80.72	80.78	63.21	94.38	78.45	82.89	80.24
PromptSRC	77.60	70.73	98.10	94.03	95.33	97.30	78.27	74.97	98.07	76.50	90.67	91.53	42.73	37.87	82.67	78.47	83.37	62.97	92.90	73.90	87.10	78.80
+ SAS	77.48	71.48	98.52	95.20	95.92	98.50	78.62	75.24	98.45	79.11	90.99	92.43	42.64	40.16	83.23	80.80	83.94	63.46	93.35	76.68	**87.66**	81.55
LASP	76.25	71.17	98.17	94.33	95.73	97.87	75.23	71.77	97.17	73.53	91.20	91.90	38.05	33.20	80.70	79.30	81.10	62.57	95.00	83.37	85.53	78.20
+ SAS	76.62	72.45	98.44	95.27	96.00	98.58	76.29	72.85	96.98	75.30	92.07	92.65	38.58	33.97	80.99	80.42	81.45	64.11	**95.61**	83.69	85.70	79.19
TCP	77.27	69.87	98.23	94.67	94.67	97.20	80.80	74.13	97.73	75.57	90.57	91.37	41.97	34.43	82.63	78.20	82.77	58.07	91.63	74.73	87.13	80.77
+ SAS	77.89	70.53	98.42	95.40	95.48	98.23	80.68	75.80	98.43	75.48	91.18	92.70	42.58	35.10	**83.41**	79.27	83.10	60.67	92.01	75.34	87.50	81.62
CLIP-Adapter	77.18	70.25	97.52	93.48	95.18	96.43	77.43	72.64	96.83	71.75	90.98	90.55	41.89	33.10	80.73	77.98	82.17	58.72	93.34	71.84	86.49	77.38
+ SAS	77.09	71.98	98.10	95.55	95.72	97.70	77.63	75.46	97.59	73.13	90.74	91.38	41.88	36.50	81.42	80.15	82.84	61.27	93.99	73.87	86.87	78.51
Tip-Adapter	78.04	71.96	98.68	94.17	96.21	98.57	80.79	73.66	98.73	74.36	92.62	91.01	**43.34**	35.73	81.77	79.27	84.58	59.91	94.82	74.81	86.78	78.94
+ SAS	77.89	72.58	**98.89**	95.72	96.65	98.43	**80.84**	75.42	**98.81**	76.73	**92.84**	92.81	43.27	38.31	82.36	80.13	**84.77**	63.38	95.51	77.54	87.42	79.77
ArGue	76.95	71.86	98.63	94.70	96.23	98.59	75.06	74.18	98.62	77.96	91.42	92.40	41.29	38.80	81.89	80.48	80.33	67.03	95.10	90.68	86.00	79.43
+ SAP	77.32	72.04	98.57	95.12	96.34	98.86	75.72	74.90	98.66	78.78	91.54	92.63	41.86	39.65	82.43	81.78	80.87	68.36	95.46	91.51	86.59	80.28
+ SAS	77.59	72.36	98.69	95.88	96.52	98.75	76.24	75.51	98.74	79.65	91.81	93.42	42.39	40.84	82.71	82.21	81.35	**69.73**	95.41	**92.47**	87.05	81.73
MAP	76.60	70.60	98.30	93.80	95.43	96.90	76.70	73.73	97.57	75.23	90.30	89.30	41.63	36.43	82.33	76.30	82.63	66.23	92.13	76.10	86.67	78.77
+ SAP	76.73	71.17	98.21	94.32	95.79	98.09	77.34	74.10	97.85	77.55	90.60	90.76	42.05	37.72	82.15	78.05	82.77	67.61	92.53	77.22	87.09	79.42
+ SAS	76.79	72.25	98.53	94.52	96.19	98.83	77.70	75.80	97.79	79.99	90.89	91.63	42.33	39.32	82.74	78.47	82.87	68.44	93.30	78.21	87.44	80.85
CPL	78.74	72.03	98.35	95.13	95.86	98.21	79.31	76.65	98.07	80.43	91.92	93.87	42.27	38.85	81.88	79.65	80.92	62.27	94.18	81.05	86.73	80.17
+ SAP	78.76	72.64	98.67	95.72	96.31	**98.87**	79.24	78.12	98.37	82.51	92.19	94.63	42.15	40.92	82.16	81.62	82.21	65.72	94.47	83.55	86.51	80.91
+ SAS	**78.82**	**73.49**	98.59	**95.98**	**96.76**	98.82	79.77	**80.35**	98.71	**83.46**	92.26	**95.45**	42.61	**41.72**	82.11	**83.17**	83.00	67.89	94.75	87.07	87.21	**82.22**

Table 25: **The numerical results on base-to-new generalization.**

	Source	Cross-dataset Transfer Target										Domain Generalization Target			
	ImageNet	Caltech	Pets	Cars	Flowers	Food	Aircraft	SUN	DTD	EuroSAT	UCF	ImageNet-V	ImageNet-S	ImageNet-A	ImageNet-R
CLIP	66.54	94.62	90.41	64.69	70.30	85.63	23.73	66.12	44.84	47.50	67.42	63.20	48.35	49.32	76.57
CoCoOp	71.02	94.43	90.14	65.32	71.88	86.06	22.94	67.36	45.73	45.37	68.21	64.07	48.75	50.63	76.18
+SAS	71.35	95.59	90.84	66.76	72.47	86.34	23.81	68.99	47.94	46.90	70.84	64.97	49.56	51.61	77.31
KgCoOp	70.66	93.92	89.83	65.41	70.01	86.36	22.51	66.16	46.35	46.04	68.50	64.10	48.97	50.69	76.70
+SAS	70.90	94.33	89.68	67.82	71.13	88.91	24.60	67.47	47.72	48.22	68.52	64.53	49.72	51.70	77.22
MaPLe	70.72	93.53	90.49	65.57	72.23	86.20	24.74	67.01	46.49	48.06	68.69	64.07	49.15	50.90	76.98
+SAS	71.21	93.61	91.76	67.53	73.60	87.58	24.54	67.69	47.98	48.17	71.96	63.98	50.74	51.57	77.25
PromptSRC	71.27	93.60	90.25	65.70	70.25	86.15	23.90	67.10	46.87	45.50	68.75	64.35	49.55	50.90	77.80
+SAS	71.53	93.25	92.60	66.44	70.13	88.19	25.05	67.87	47.22	45.50	68.99	64.07	50.40	51.52	**78.98**
LASP	71.34	93.65	91.83	67.29	70.82	88.54	28.60	65.75	54.83	43.65	69.23	64.04	47.93	49.11	75.36
+SAS	71.62	94.62	92.98	68.89	71.18	89.89	29.68	68.47	55.74	45.80	71.63	65.24	47.91	50.80	77.08
TCP	71.40	93.97	91.25	64.69	71.21	86.69	23.45	67.15	44.35	51.45	68.73	64.60	49.50	51.20	76.73
+SAS	71.73	94.73	92.60	66.54	71.44	87.81	24.80	68.94	45.15	52.93	70.31	65.62	50.79	**52.94**	78.82
CLIP-Adapter	72.35	93.06	90.76	63.17	69.23	85.13	20.54	65.57	43.27	49.64	66.33	62.91	49.15	51.74	76.81
+SAS	72.53	93.12	91.72	66.65	69.18	88.10	22.27	66.60	45.69	50.38	69.80	64.50	49.70	52.39	77.75
Tip-Adapter	72.53	95.71	93.12	66.61	68.83	89.22	23.63	68.32	47.31	53.40	68.15	63.30	49.26	50.18	76.70
+SAS	72.81	95.49	**94.88**	67.80	68.46	91.77	25.00	69.46	49.55	**54.33**	68.94	64.21	50.34	50.89	77.93
ArGue	71.84	94.20	92.66	70.70	71.29	91.64	28.28	70.51	55.37	45.76	71.97	65.02	49.25	51.47	76.96
+SAP	72.14	95.74	93.75	71.80	72.48	91.87	28.53	70.88	56.54	46.86	72.96	65.47	49.94	52.48	77.38
+SAS	72.28	95.67	94.29	**72.72**	74.63	**92.53**	29.10	**71.96**	**57.40**	48.22	**73.82**	66.12	49.90	52.85	77.90
MAP	71.60	93.93	90.80	63.00	68.40	86.07	24.87	68.10	51.87	42.63	68.73	64.47	49.07	51.07	77.37
+SAP	71.93	95.40	92.63	64.50	68.13	87.18	26.80	69.99	51.35	44.10	70.50	65.06	49.88	51.64	77.34
+SAS	72.21	95.82	93.73	66.69	68.46	88.11	28.62	70.29	51.91	45.73	71.59	66.14	50.78	52.19	77.70
CPL	73.53	95.52	91.64	66.17	73.35	87.68	27.36	68.24	48.96	51.25	70.52	65.24	50.84	52.10	76.76
+SAP	73.75	**95.83**	92.92	66.69	74.32	88.33	29.58	69.64	49.81	52.72	71.35	**66.45**	51.93	52.61	77.74
+SAS	**73.94**	95.74	93.67	67.22	**75.67**	89.49	**30.55**	70.26	49.91	54.29	72.48	66.38	**52.95**	52.81	78.31

Table 26: **The numerical results on cross-dataset transfer and domain generalization.**

REFERENCES

Dyah Adila, Changho Shin, Linrong Cai, and Frederic Sala. Zero-shot robustification of zero-shot models with foundation models. In *ICLR*, 2023.

Zhe Chen, Jiannan Wu, Wenhai Wang, Weijie Su, Guo Chen, Sen Xing, Muyan Zhong, Qinglong Zhang, Xizhou Zhu, Lewei Lu, et al. Internvl: Scaling up vision foundation models and aligning for generic visual-linguistic tasks. In *CVPR*, pp. 24185–24198, 2024.

Mircea Cimpoi, Subhransu Maji, Iasonas Kokkinos, Sammy Mohamed, and Andrea Vedaldi. Describing textures in the wild. In *CVPR*, pp. 3606–3613. IEEE Computer Society, 2014.

Jia Deng, Wei Dong, Richard Socher, Li-Jia Li, Kai Li, and Li Fei-Fei. Imagenet: A large-scale hierarchical image database. In *CVPR*, pp. 248–255. IEEE Computer Society, 2009.

Li Fei-Fei, Rob Fergus, and Pietro Perona. Learning generative visual models from few training examples: An incremental bayesian approach tested on 101 object categories. In *CVPR Workshops*, pp. 178. IEEE Computer Society, 2004.

Raghav Goyal, Samira Ebrahimi Kahou, Vincent Michalski, Joanna Materzynska, Susanne Westphal, Heuna Kim, Valentin Haenel, Ingo Fruend, Peter Yianilos, Moritz Mueller-Freitag, et al. The" something something" video database for learning and evaluating visual common sense. In *ICCV*, pp. 5842–5850, 2017.

Patrick Helber, Benjamin Bischke, Andreas Dengel, and Damian Borth. Eurosat: A novel dataset and deep learning benchmark for land use and land cover classification. *IEEE J. Sel. Top. Appl. Earth Obs. Remote. Sens.*, 12(7):2217–2226, 2019.

Dan Hendrycks, Kevin Zhao, Steven Basart, Jacob Steinhardt, and Dawn Song. Natural adversarial examples. In *CVPR*, pp. 15262–15271. Computer Vision Foundation / IEEE, 2021.

Will Kay, Joao Carreira, Karen Simonyan, Brian Zhang, Chloe Hillier, Sudheendra Vijayanarasimhan, Fabio Viola, Tim Green, Trevor Back, Paul Natsev, et al. The kinetics human action video dataset. *arXiv preprint arXiv:1705.06950*, 2017.

Muhammad Uzair Khattak, Hanoona Abdul Rasheed, Muhammad Maaz, Salman H. Khan, and Fahad Shahbaz Khan. Maple: Multi-modal prompt learning. In *CVPR*, pp. 19113–19122. IEEE, 2023a.

Muhammad Uzair Khattak, Syed Talal Wasim, Muzammal Naseer, Salman Khan, Ming-Hsuan Yang, and Fahad Shahbaz Khan. Self-regulating prompts: Foundational model adaptation without forgetting. In *ICCV*, pp. 15190–15200, 2023b.

Alexander Kirillov, Eric Mintun, Nikhila Ravi, Hanzi Mao, Chloe Rolland, Laura Gustafson, Tete Xiao, Spencer Whitehead, Alexander C Berg, Wan-Yen Lo, et al. Segment anything. In *CVPR*, pp. 4015–4026, 2023.

Jonathan Krause, Michael Stark, Jia Deng, and Li Fei-Fei. 3d object representations for fine-grained categorization. In *ICCV Workshops*, pp. 554–561. IEEE Computer Society, 2013.

Alex Krizhevsky, Geoffrey Hinton, et al. Learning multiple layers of features from tiny images. *NA*, 2009.

Hildegard Kuehne, Hueihan Jhuang, Estíbaliz Garrote, Tomaso Poggio, and Thomas Serre. Hmdb: a large video database for human motion recognition. In *ICCV*, pp. 2556–2563. IEEE, 2011.

Junnan Li, Dongxu Li, Caiming Xiong, and Steven Hoi. Blip: Bootstrapping language-image pre-training for unified vision-language understanding and generation. In *ICML*, 2022.

Junnan Li, Dongxu Li, Silvio Savarese, and Steven Hoi. Blip-2: Bootstrapping language-image pre-training with frozen image encoders and large language models. In *ICML*, pp. 19730–19742. PMLR, 2023.

Xianhang Li, Zeyu Wang, and Cihang Xie. An inverse scaling law for clip training. In *NeurIPS*, volume 36, 2024.

Haotian Liu, Chunyuan Li, Qingyang Wu, and Yong Jae Lee. Visual instruction tuning. In *NeurIPS*, volume 36, 2024.

Ziwei Liu, Ping Luo, Xiaogang Wang, and Xiaoou Tang. Large-scale celebfaces attributes (celeba) dataset. *Retrieved August*, 15(2018):11, 2018.

Alexander Long, Wei Yin, Thalaiyasingam Ajanthan, Vu Nguyen, Pulak Purkait, Ravi Garg, Alan Blair, Chunhua Shen, and Anton van den Hengel. Retrieval augmented classification for long-tail visual recognition. In *CVPR*, pp. 6959–6969, 2022.

Andreas Lugmayr, Martin Danelljan, Andres Romero, Fisher Yu, Radu Timofte, and L Repaint Van Gool. Inpainting using denoising diffusion probabilistic models. In *CVPR*, pp. 11461–11471, 2022.

Sachit Menon and Carl Vondrick. Visual classification via description from large language models. In *ICLR*. OpenReview.net, 2023.

Shubham Parashar, Zhiqiu Lin, Tian Liu, Xiangjue Dong, Yanan Li, Deva Ramanan, James Caverlee, and Shu Kong. The neglected tails of vision-language models. In *CVPR*, 2024.

Omkar M. Parkhi, Andrea Vedaldi, Andrew Zisserman, and C. V. Jawahar. Cats and dogs. In *CVPR*, pp. 3498–3505. IEEE Computer Society, 2012.

Sarah Pratt, Ian Covert, Rosanne Liu, and Ali Farhadi. What does a platypus look like? generating customized prompts for zero-shot image classification. In *ICCV*, pp. 15691–15701, 2023.

Alec Radford, Jong Wook Kim, Chris Hallacy, Aditya Ramesh, Gabriel Goh, Sandhini Agarwal, Girish Sastry, Amanda Askell, Pamela Mishkin, Jack Clark, Gretchen Krueger, and Ilya Sutskever. Learning transferable visual models from natural language supervision. In *ICML*, volume 139 of *Proceedings of Machine Learning Research*, pp. 8748–8763. PMLR, 2021.

Hanoona Rasheed, Muhammad Uzair Khattak, Muhammad Maaz, Salman Khan, and Fahad Shahbaz Khan. Fine-tuned clip models are efficient video learners. In *CVPR*, pp. 6545–6554, 2023.

Robin Rombach, Andreas Blattmann, Dominik Lorenz, Patrick Esser, and Björn Ommer. High-resolution image synthesis with latent diffusion models. In *CVPR*, 2022.

Shiori Sagawa, Pang Wei Koh, Tatsunori B Hashimoto, and Percy Liang. Distributionally robust neural networks for group shifts: On the importance of regularization for worst-case generalization. *arXiv preprint arXiv:1911.08731*, 2019.

Shibani Santurkar, Dimitris Tsipras, and Aleksander Madry. Breeds: Benchmarks for subpopulation shift. In *ICLR*, 2020.

Christoph Schuhmann, Romain Beaumont, Richard Vencu, Cade Gordon, Ross Wightman, Mehdi Cherti, Theo Coombes, Aarush Katta, Clayton Mullis, Mitchell Wortsman, et al. Laion-5b: An open large-scale dataset for training next generation image-text models. In *NeurIPS*, 2022.

Julio Silva-Rodriguez, Sina Hajimiri, Ismail Ben Ayed, and Jose Dolz. A closer look at the few-shot adaptation of large vision-language models. In *CVPR*, pp. 23681–23690, 2024.

Sahil Singla and Soheil Feizi. Salient imagenet: How to discover spurious features in deep learning? In *ICLR*, 2021.

K Soomro. Ucf101: A dataset of 101 human actions classes from videos in the wild. *arXiv preprint arXiv:1212.0402*, 2012.

Quan Sun, Yuxin Fang, Ledell Wu, Xinlong Wang, and Yue Cao. Eva-clip: Improved training techniques for clip at scale. *arXiv preprint arXiv:2303.15389*, 2023.

Xinyu Tian, Shu Zou, Zhaoyuan Yang, and Jing Zhang. Argue: Attribute-guided prompt tuning for vision-language models. In *CVPR*, 2024.

Vishaal Udandarao, Ankush Gupta, and Samuel Albanie. Sus-x: Training-free name-only transfer of vision-language models. In *ICCV*, 2022.

Eric Wong, Shibani Santurkar, and Aleksander Madry. Leveraging sparse linear layers for debuggable deep networks. In *ICML*, pp. 11205–11216, 2021.

Shirley Wu, Mert Yuksekgonul, Linjun Zhang, and James Zou. Discover and cure: Concept-aware mitigation of spurious correlation. In *ICML*, pp. 37765–37786. PMLR, 2023.

Lingxiao Yang, Ru-Yuan Zhang, Yanchen Wang, and Xiaohua Xie. Mma: Multi-modal adapter for vision-language models. In *CVPR*, pp. 23826–23837, 2024.

Hantao Yao, Rui Zhang, and Changsheng Xu. Tcp: Textual-based class-aware prompt tuning for visual-language model. In *CVPR*, 2024.

Chenyu You, Yifei Mint, Weicheng Dai, Jasjeet S Sekhon, Lawrence Staib, and James S Duncan. Calibrating multi-modal representations: A pursuit of group robustness without annotations. In *CVPR*, pp. 26140–26150. IEEE, 2024.

Xiaohua Zhai, Basil Mustafa, Alexander Kolesnikov, and Lucas Beyer. Sigmoid loss for language image pre-training. In *ICCV*, pp. 11975–11986, 2023.

Michael Zhang and Christopher Ré. Contrastive adapters for foundation model group robustness. In *NeurIPS*, volume 35, pp. 21682–21697, 2022.

Yabin Zhang, Wenjie Zhu, Hui Tang, Zhiyuan Ma, Kaiyang Zhou, and Lei Zhang. Dual memory networks: A versatile adaptation approach for vision-language models. In *CVPR*, pp. 28718–28728, 2024a.

Yi Zhang, Ce Zhang, Ke Yu, Yushun Tang, and Zhihai He. Concept-guided prompt learning for generalization in vision-language models. In *AAAI*, 2024b.

Kaiyang Zhou, Jingkang Yang, Chen Change Loy, and Ziwei Liu. Learning to prompt for vision-language models. *IJCV*, 130(9):2337–2348, 2022a.

Kaiyang Zhou, Jingkang Yang, Chen Change Loy, and Ziwei Liu. Conditional prompt learning for vision-language models. In *CVPR*, pp. 16795–16804. IEEE, 2022b.